APL Materials

RESEARCH ARTICLE | DECEMBER 20 2021

Mid-infrared cylindrical vector beams enabled by dielectric metasurfaces

Anastasia Zalogina ; Luyao Wang; Elizaveta Melik-Gaykazyan ; Yuri Kivshar; Ilya Shadrivov ; Sergey Kruk

APL Mater 9, 121113 (2021)
https://doi.org/10.1063/5.0061825

Mid-infrared cylindrical vector beams enabled by dielectric metasurfaces

Cite as: APL Mater. 9, 121113 (2021); doi: 10.1063/5.0061825
Submitted: 30 June 2021 • Accepted: 9 November 2021 •
Published Online: 20 December 2021

Anastasia Zalogina,[a] Luyao Wang, Elizaveta Melik-Gaykazyan, Yuri Kivshar, Ilya Shadrivov, and Sergey Kruk

AFFILIATIONS

Nonlinear Physics Centre, Research School of Physics, Australian National University, Canberra ACT 2601, Australia

Note: This paper is part of the Special Topic on Light and Matter Interactions.
[a]**Author to whom correspondence should be addressed:** anastasiia.zalogina@anu.edu.au

ABSTRACT

Over the last decade, photonics in the mid-infrared (mid-IR) frequency range had major advances in both generation and detection of light. However, efficient manipulation of the mid-IR light still faces many challenges. Spatially inhomogeneous control over the wavefront and polarization of mid-IR radiation is particularly difficult. Many standard techniques used for visible and near-infrared frequencies, such as liquid crystal-based spatial light modulation, are not applicable in the mid-IR due to unfavorable material properties in that spectral range. Here, we demonstrate spatially inhomogeneous polarization control of the mid-infrared light using custom-designed vortex retarders. Vortex retarders, while being widely used in the near-infrared and visible spectral ranges for generation of cylindrical vector beams, have been missing in the mid-infrared spectral range. Our implementation of mid-infrared vortex retarders is based on the concept of metasurfaces. We demonstrate metasurface-based vortex retarders at the wavelengths of 2.9 and 3.5 μm. We compare the performance of all-dielectric metasurface vortex retarders with the elements arranged in square and hexagonal lattices [Arbabi *et al.*, Nat. Nanotechnol. **10**, 937–943 (2015) and Arbabi *et al.*, Nat. Commun. **6**, 7069 (2015)]. Our work could accelerate the adoption of metasurfaces for the development of novel classes of mid-infrared optical components.

I. INTRODUCTION

The mid-infrared (mid-IR) band from 2.5 to 10 μm has strategic significance in photonics because it hosts absorption bands of biochemicals, as well as two atmospheric windows of transparency. The mid-IR optics and photonics find their applications in spectroscopy,[3,4] chemical and biological sensing[5,6] and imaging,[7] and free-space communications[8] among others. Although photonics' success in the mid-IR was envisioned some time ago,[9] mid-IR technology struggles to catch up with its counterparts in the visible and near-infrared (near-IR) spectral ranges.[10–12]

The development of photonic devices in the mid-IR spectral range is often met with significant challenges associated with the need for unconventional materials and the limited choice of optical components. Traditional manufacturing of visible and near-infrared optical components is often not transferable to the mid-IR spectral region as many common optical materials, such as silicate glass, optical polymers, and liquid crystals, become opaque. A class of components widely used in the visible and near-IR spectral ranges, but largely missing in the mid-IR, is associated with spatially inhomogeneous control of polarization of light. Complex polarization patterns, often termed "vector beams," as well as polarization singularities find numerous applications in contemporary photonics.[13–17] Such beams are of particular practical importance in various technological advances including optical trapping,[18,19] biosensing,[20,21] and nonlinear optics.[22,23] Vector beams are solutions of Maxwell's equations, and cylindrical vector beams can be decomposed into radial and azimuthal polarized modes, as a superposition of orthogonally polarized Hermite–Gauss HG_{01} and HG_{10} modes.[24] The electric field at the focus of a cylindrical vector beam has unique polarization properties due to this symmetry. For example, the longitudinal component of the field in the focus of such a cylindrical beam can be much stronger than the transverse component, and the size of the longitudinal focus is much smaller than the transverse one.

Creation of complex polarization patterns, such as cylindrical vector beams in the visible and near-IR spectral ranges, conventionally relies on spatial light modulators and other liquid crystal-

based technologies that are not applicable to wavelengths past 3 μm. Other methods for the generation of cylindrical vector beams include Brewster angle reflectors,[25] mirror devices,[26] and Sagnac interferometer.[27] These are often termed "active methods" as they involve amplifying media and therefore they are not immediately applicable in the mid-IR range. Radial analyzers[28] and spiral phase elements[29] are examples of passive methods. However, all the above approaches have conventionally been used in the visible and near-IR spectral ranges.

A viable alternative pathway toward complex manipulations of mid-IR comes from the area of dielectric metasurfaces. Metasurfaces have attracted enormous attention as their optical properties can be designed on demand.[1,2,30–33] Extension of the concept of metasurfaces into the mid-IR spectral band provides a powerful platform for future optical devices with enhanced performance. Originally, many applications have been proposed based on metasurfaces made of metals. However, low efficiency caused by Ohmic losses has limited the practicality of metal-based metasurfaces.[34] In recent years, high refractive index dielectric metasurfaces have emerged as an efficient alternative.

All-dielectric metasurfaces supporting both strong electric and magnetic Mie-type resonances are capable of controlling virtually every parameter of electromagnetic waves. This is achieved via judicious engineering of the size, geometric shape, and spatial orientation of their constituent elements. Metasurfaces made of high-index nanopillars placed on low-index substrates were proven to work as functional components in the visible and near-infrared spectral ranges[1,2,35] often outperforming more conventional optical components while offering a nanoscale form factor. Individual pillars within the metasurface can be optimized for high forward scattering, keeping backward scattering and absorption low, so that an array of such pillars is transparent for the incident radiation. This is achieved via the generalized Huygens principle.[35] High efficiency of both phase and polarization control has been demonstrated with such metasurfaces.

Here, we employ the all-dielectric metasurfaces for mid-infrared phonics applications. We design metasurface vortex retarders based on a combination of materials with favorable properties in the mid-infrared spectral range. We report on fabrication protocols and on optical diagnostics results for the retarders operating at two wavelengths of interest, i.e., at 2.9 and 3.5 μm. Our metasurfaces are made of arrays of silicon subwavelength pillars on a sapphire substrate. Both silicon and sapphire feature low material absorption in the mid-infrared spectral range. This pair of materials further has a high contrast of their refractive indices desirable for the metasurface design. Each individual pillar acts as a half-wave plate locally rotating the incident polarization, with the polarization rotation angle being controlled by the pillar's orientation.[35] The

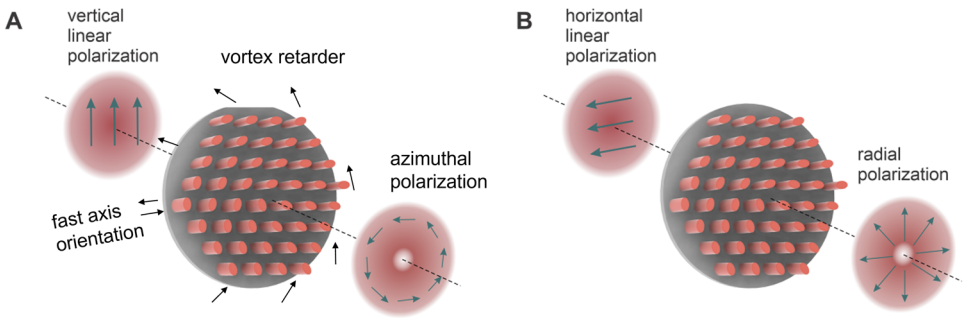

FIG. 1. Conceptual image of the vector beam transformation with the help of mid-IR metasurface-based vortex retarders (also known as *q*-plates) allowing us to generate either (a) azimuthally polarized vector beam or (b) radially polarized vector beam. Black arrows in (a) indicate the fast axis orientation.

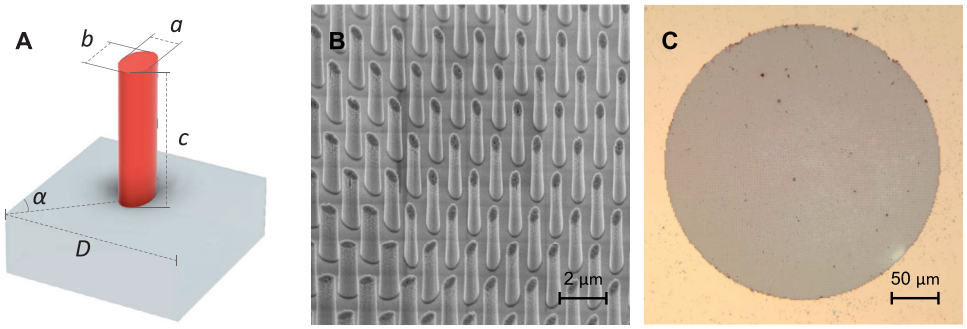

FIG. 2. (a) Schematic of a single pillar with the following dimensions: minor diameter *a* is 0.47 μm, major diameter *b* is 0.755 μm, height *c* is 1.9 μm, period *D* is 1.729 μm, and unit cell angle α is 60° (in the case of a hexagonal lattice). (b) Scanning electron microscope image of the fabricated metasurface. (c) Optical microscope image of the fabricated metasurface.

overall layout of the pillars features a topological charge factor of 0.5 shaping a linearly polarized Gaussian beam into azimuthally or radially polarized beams with Bessel–Gaussian amplitude distribution (Fig. 1).

II. DESIGN APPROACH

We design the metasurfaces using commercially available software CST Studio Suite 2020 and COMSOL Multiphysics version 5.5. Figure 2(a) provides the details of the resulting set of the design parameters for the constituent subwavelength pillar element optimized for 2.9 μm wavelength. To simplify the model, we numerically simulate half-wave plates, where all modeled pillars have the same orientation. The calculated results are presented in Figs. 3(a) and 4(a). In our design, the direction of the optical axis of the element on the vortex retarder $\theta(x, y)$ can be expressed as

$$\theta(x, y) = q\varphi, \tag{1}$$

where q is the topological charge of the vortex retarder, representing the number of rotations of the local optical axis around the center of the plate, and φ is the angular coordinate in the cylindrical coordinate system linked to Cartesian coordinates as $\varphi = \tan^{-1}(y/x)$. Figure 1 visualizes polarization transformations performed by the vortex retarder metasurface. The output light field can be expressed as

$$\vec{E}_{out}(x, y) = \vec{E}_0(x, y)\begin{bmatrix}\cos(2q\theta - \theta_0)\\ \sin(2q\theta - \theta_0)\end{bmatrix}. \tag{2}$$

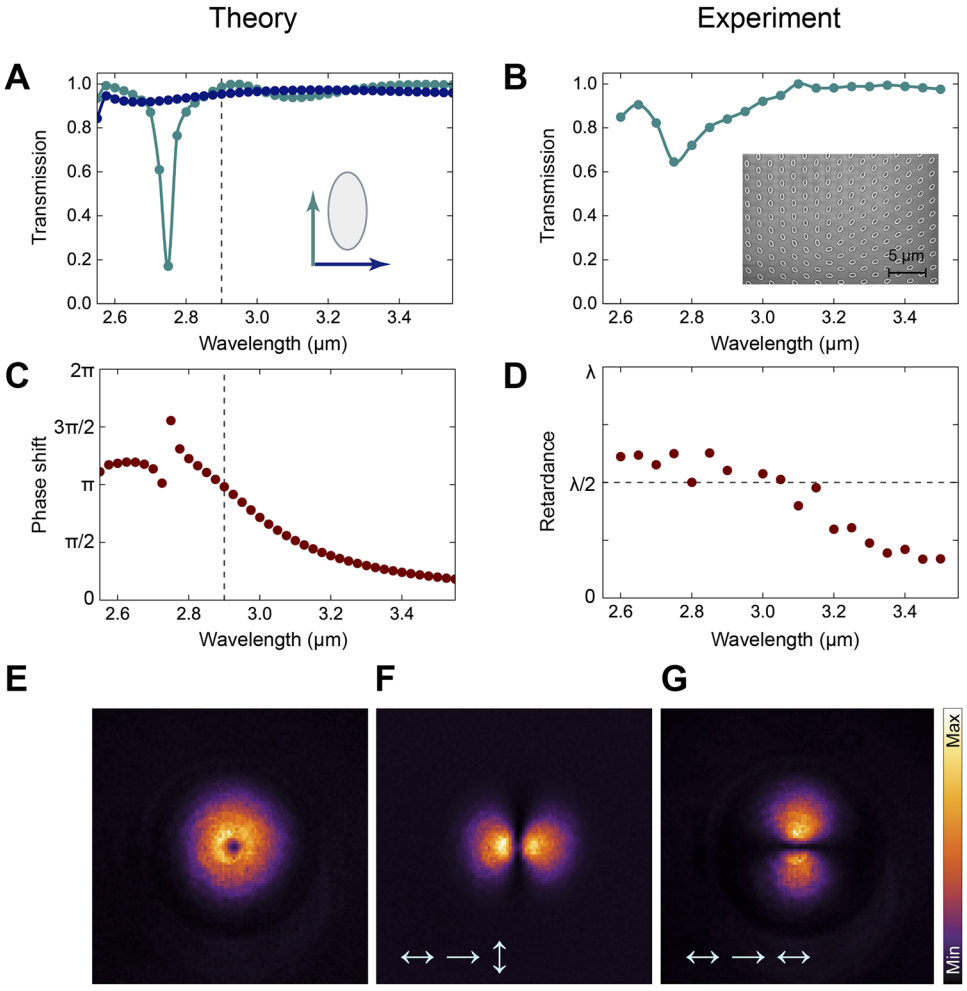

FIG. 3. Theoretical and experimental results for a metasurface of a hexagonal lattice. (a) Calculated transmission spectra of the metasurface of linearly polarized light. The green and blue arrows indicate the polarization directions along the long and short axes of a pillar accordingly. (b) Measured transmission spectra of linearly polarized light through the metasurface. Inset: scanning electron microscope image of the fabricated metasurface acting at 2.9 μm. (c) Calculated phase shift of two orthogonal components of the electric field passing through the metasurface segment. (d) Retardance of the fabricated metasurface retrieved from the experimental data. (e) Experimental intensity profile of the transmitted beam hosting a polarization singularity. (f) and (g) Light transmission through the vortex retarder metasurface positioned between a polarizer and an analyzer at 2.9 μm. Orientations of the polarizer and the analyzer are shown as inset arrows.

Thus, the output polarization state (radial, azimuthal, or intermediate) is determined by the polarization angle of the incident light. When the angle between the incident polarization direction and the vortex retarder axis $\theta_0 = 0$, the output light is radially polarized and when $\theta_0 = \pi/2$, the output light is azimuthally polarized. Based on the above condition, the structure is designed in such a way that the phase difference for two orthogonal linear polarizations is 0.5π. The parameters that are achieved by this condition are presented in Fig. 1(a).

III. FABRICATION METHODS

To fabricate the designed vortex retarder, first, a 2 μm amorphous silicon (α-Si) thin film is deposited on a sapphire wafer using the plasma chemical vapor deposition system Temescal BJD-2000. The thickness is measured using the ellipsometer JA Woollam M-2000D. Then, a 200 nm e-beam resist CSAR 62 (AR-P 6200-09) is deposited using a spinner. Since the sample is made of semiconductor and dielectric materials, a conductive layer Electra 92 (AR-PC 5090.02) is deposited at the top of the resist for the dissipation of charges during electron beam exposure. The metasurface pattern on the sample is defined by exposing it in the electron beam lithography setup (Elionix ELS-F125), with the area dose of the electron beam exposure of 360 μAs/cm^2. Next, the mask is formed by depositing 40 nm of aluminum using the electron beam evaporation system AJA ATC-1800-E and subsequent lift-off process at 80 °C using NMP (1-methyl-2-pyrrolidone). The metasurface pattern is transferred onto the material using an inductively coupled plasma reactive ion etching (Oxford ICP-RIE Plasmalab 100) with C_4F_8 and SF_6 gases. Finally, the aluminum mask is removed with wet etching using orthophosphoric acid of 85% concentration.

Electron microscope images of the resulting samples were obtained using a field emission scanning electron microscope Verios scanning electron microscope. The resulting two fabricated metasurfaces consist of silicon ellipses of 2.0 μm height, 0.72 μm large diameter, and 0.42 μm small diameter, the period of 1.695 μm, and the ellipse rotation of 0.5.

The imperfections of fabrication are the result from physical defects of electron-beam exposure, such as dose error, and from over-etching of silicon, where the sizes of ellipses would be a bit smaller or larger than expected.

IV. RESULTS AND DISCUSSION

In the optical experiment, the linearly polarized light is converted into spatially non-uniformly polarized light by a fabricated vortex retarder with spatial polarization characteristics, where the spatially variable polarization rotation and the spatially variable retardation axis arrangement are used. Because the polarization direction is dependent on the spatial coordinates, the spatial distribution of the vortex retarder's optical axis is designed to manipulate the polarization distribution. The designed structure is characterized by the phase difference of 0.5π, so when the angle between the incident polarization and the vortex retarder axis is 0.5π, the transmitted light through the vortex retarder is azimuthally polarized.

The vortex retarder is illuminated by a light beam from a tunable mid-IR laser polarized linearly. The vortex retarder is placed on a rotating mount that allows us to alter the polarization of the output beam between radial and azimuthal. An analyzer is used to measure the spatially resolved Stokes parameters of the light field on the CCD camera retrieving polarization states across the output cylindrical vector beams. With a pulse duration of 2 ps, it has an output wavelength of 1030 nm and a repetition rate of 5 MHz. By passing it through an optical parametric amplifier, signal and idler beams are produced, which allows us to conduct mid-IR spectroscopy in the range of 2.5–4.0 μm.

The experimental results for the fabricated vortex retarder acting at 2.9 μm are shown in Figs. 3(b), 3(d), and 3(e)–3(g). The results of the corresponding numerical calculations are shown in Figs. 3(a) and 3(c). Figure 3(b) shows the resulting transmission of the fabricated vortex retarder. The difference between theoretical [Fig. 3(a)] and experimental [Fig. 3(b)] results occurs mostly because of the fabrication imperfections, where the walls of pillars can be slightly tapered, some geometrical parameters are offset, or the refractive index is deviated. Figure 3(d) contains the retrieved retardance of the metasurface. The retardance was extracted via polarimetry using a standard method[36] for which a small segment of the metasurface acting as a half-wave plate was inspected. The entire metasurface

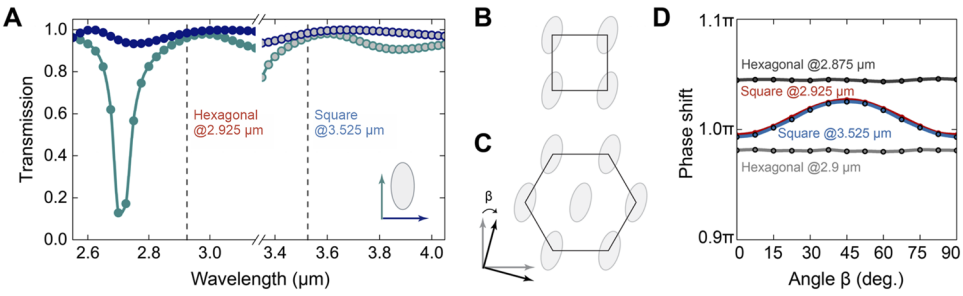

FIG. 4. Comparison of square and hexagonal lattices for a half-wave plate metasurface performance. (a) Calculated transmission spectra of a linearly polarized light of two orthogonal polarizations passing through a metasurface with a square unit cell. The green and blue arrows indicate the polarization directions along the long and short axes of a pillar accordingly. The results for two designs are shown: $c = 1.61$, $a = 0.534$, $b = 0.842$, $D = 1.405$ μm, $\alpha = 45°$ (design 1, filled circles) and $c = 1.94$, $a = 0.645$, $b = 1.017$, $D = 1.692$ μm, $\alpha = 45°$ (design 2, gray circles). (b) and (c) Schematics of the rotation of pillar axes relative to (b) a square and (c) a hexagonal unit cell. (d) Angular dependence of a phase shift on the orientation of a pillar and x–y axes in relation to a unit cell: hexagonal unit cell at 2.875 μm (dark gray) and at 2.9 μm (light gray); square unit cell of the first design at 2.925 μm (red) and the second design at 3.525 μm (blue).

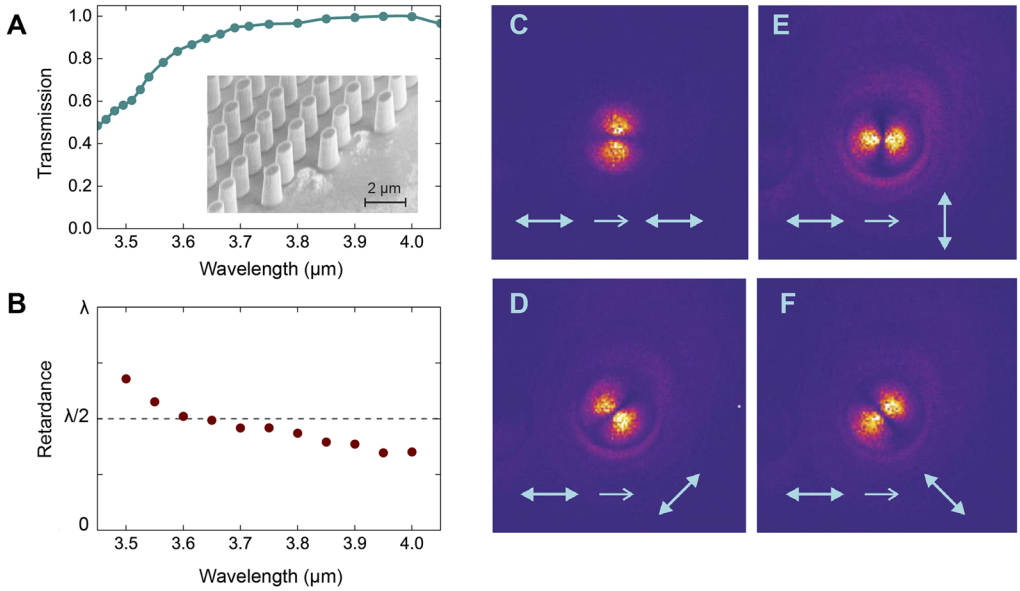

FIG. 5. Experimental results for a metasurface of a square lattice. (a) Measured transmission spectra of linearly polarized light passed through a vortex retarder. The inset shows a scanning electron microscopy image of the fabricated metasurface with the following parameters: $a = 0.706$, $b = 1.051$, $c = 1.94$, $D = 1.692$ μm, and $\alpha = 45°$. (b) Retardance retrieved from polarimetry measurements. (c)–(f) Polarimetry images: light transmission through the vortex retarder positioned between a polarizer and an analyzer at 3.5 μm. The polarizer state is horizontal, states of the analyzer: (c) horizontal, (e) vertical, and (d) and (f) diagonal, correspondingly.

creates a cylindrical vector beam as shown in Figs. 3(e)–3(g). The special arrangement of the pillars is shown in Fig. 2(b). Spatially inhomogeneous distribution of optical axes of pillars creates the polarization that depends on in-plane spatial coordinates, and the resulting output beams have the shape of cylindrical vector beams.

We further compare vortex retarders with a hexagonal lattice and retarders with a square lattice. We demonstrate that the higher rotational symmetry of the hexagonal lattice leads to a more precise and smooth polarization control of the incident beam. We also model a half-wave plate metasurface based on a square unit cell working at around the wavelength of 3.5 μm. The high transmission can be also realized in this case as depicted in Fig. 4(a), which is also confirmed experimentally for the hexagonal lattice in Fig. 3(b) and for the square lattice in Fig. 5. However, when the pillars are rotated for generating spatially resolved phase shift distributions, the performance of square unit cells degrades. In order to demonstrate this, we perform calculations of the dependence of a phase shift on the angle of a pillar orientation in a unit cell, see Fig. 4(d). In these simulations, we always consider the electric field components as aligned to minor and major axes of a unit cell ellipse.

Finally, we fabricate the second vortex retarder based on a square-lattice metasurface with the working spectral range optimized in the vicinity of 3.5 μm. Our experimental results are summarized in Fig. 5, which shows the measured transmission spectra of linearly polarized light passed through the vortex retarder, as well as retardance retrieved from polarimetry measurements, together with the polarimetry images. The images showing polarimetry measurements in Figs. 5(e) and 5(f) have a bright halo. This can be an inadvertent glare where light is passing outside of the metasurface due to imperfections in our illumination scheme.

V. CONCLUSION

We have designed and fabricated metasurface-based mid-IR vortex retarders for two on-demand wavelengths of 2.9 and 3.5 μm. Our all-dielectric metasurfaces are composed of elliptically shaped subwavelength pillars with overall layout featuring a topological charge factor of 0.5 shaping a linearly polarized Gaussian beam into azimuthally or radially polarized vector beams with the Bessel–Gaussian amplitude distribution. We have achieved both high transmission and high polarization conversion efficiencies by engineering the shape and size of the subwavelength elements. We have compared the metasurface layouts with square and hexagonal lattices and demonstrated superior performance of the hexagonal lattice due to its higher rotational symmetry. Our results enable a flexible approach for the design and fabrication of larger classes of metasurface-based optical components for spatially inhomogeneous control of polarization of light in the mid-infrared spectral range. The work demonstrates the potential of all-dielectric metasurfaces to provide cutting-edge optical devices for mid-IR photonics.

ACKNOWLEDGMENTS

The authors acknowledge the use of the fabrication facilities as well as scientific and technical assistance from the Research and Prototype Foundry Core Research Facility at the University of Sydney, being a part of the Australian National Fabrication Facility, and the ACT node of the NCRIS-enabled Australian National Fabrication Facility (ANFF-ACT). Sergey Kruk acknowledges the support from the Australian Research Council (Grant No. DE210100679). Yuri Kivshar acknowledges the support from the Australian Research

Council (Grant Nos. DP200101168 and DP210101292) and the U.S. Army International Office (Grant No. FA520921P0034).

AUTHOR DECLARATIONS

Conflict of Interest

The authors have no conflicts to disclose.

Author Contributions

A.Z., L.W., and E.M.-G. contributed equally to this work.

DATA AVAILABILITY

The data that support the findings of this study are available from the corresponding author upon reasonable request.

REFERENCES

[1]A. Arbabi, Y. Horie, M. Bagheri, and A. Faraon, "Dielectric metasurfaces for complete control of phase and polarization with subwavelength spatial resolution and high transmission," Nat. Nanotechnol. **10**, 937–943 (2015).
[2]A. Arbabi, Y. Horie, A. J. Ball, M. Bagheri, and A. Faraon, "Subwavelength-thick lenses with high numerical apertures and large efficiency based on high-contrast transmitarrays," Nat. Commun. **6**, 7069 (2015).
[3]N. Picqué and T. W. Hänsch, "Frequency comb spectroscopy," Nat. Photonics **13**, 146–157 (2019).
[4]G. M. Smolik, N. Descharmes, and H. P. Herzig, "Toward Bloch surface wave-assisted spectroscopy in the mid-infrared region," ACS Photonics **5**, 1164–1170 (2018).
[5]E. Mohammadi and N. Behdad, "A wide dynamic range polarization sensing long wave infrared detector," Sci. Rep. **7**, 17475 (2017).
[6]J. Martínez, A. Ródenas, M. Aguiló, T. Fernandez, J. Solis, and F. Díaz, "Mid-infrared surface plasmon polariton chemical sensing on fiber-coupled ito coated glass," Opt. Lett. **41**, 2493–2496 (2016).
[7]L. Tong, X. Huang, P. Wang, L. Ye, M. Peng, L. An, Q. Sun, Y. Zhang, G. Yang, Z. Li *et al.*, "Stable mid-infrared polarization imaging based on quasi-2D tellurium at room temperature," Nat. Commun. **11**, 2308 (2020).
[8]V. Vakarin, J. Ramírez, J. Frigerio, Q. Liu, A. Ballabio, X. Le Roux, C. Alonso-Ramos, G. Isella, P. Cheben, W. N. Ye *et al.*, "Wideband Ge-rich SiGe polarization-insensitive waveguides for mid-infrared free-space communications," Appl. Sci. **8**, 1154 (2018).
[9]R. Soref, "Mid-infrared photonics in silicon and germanium," Nat. Photonics **4**, 495–497 (2010).
[10]S. Dixit, N. R. Sahoo, A. Mall, and A. Kumar, "Mid infrared polarization engineering via sub-wavelength biaxial hyperbolic van der Waals crystals," Sci. Rep. **11**, 6612 (2021).
[11]Y. Fang, Y. Ge, C. Wang, and H. Zhang, "Mid-infrared photonics using 2D materials: Status and challenges," Laser Photonics Rev. **14**, 1900098 (2020).
[12]S. Law, V. Podolskiy, and D. Wasserman, "Towards nano-scale photonics with micro-scale photons: The opportunities and challenges of mid-infrared plasmonics," Nanophotonics **2**, 103–130 (2013).
[13]Q. Zhan, "Cylindrical vector beams: From mathematical concepts to applications," Adv. Opt. Photonics **1**, 1–57 (2009).
[14]J. Kindler, P. Banzer, S. Quabis, U. Peschel, and G. Leuchs, "Waveguide properties of single subwavelength holes demonstrated with radially and azimuthally polarized light," Appl. Phys. B **89**, 517–520 (2007).
[15]P. Banzer, U. Peschel, S. Quabis, and G. Leuchs, "On the experimental investigation of the electric and magnetic response of a single nano-structure," Opt. Express **18**, 10905–10923 (2010).
[16]G. Bautista and M. Kauranen, "Vector-field nonlinear microscopy of nanostructures," ACS Photonics **3**, 1351–1370 (2016).
[17]T. Das, P. P. Iyer, R. A. DeCrescent, and J. A. Schuller, "Beam engineering for selective and enhanced coupling to multipolar resonances," Phys. Rev. B **92**, 241110 (2015).
[18]H. Moradi, V. Shahabadi, E. Madadi, E. Karimi, and F. Hajizadeh, "Efficient optical trapping with cylindrical vector beams," Opt. Express **27**, 7266–7276 (2019).
[19]N. Bhebhe, P. A. C. Williams, C. Rosales-Guzmán, V. Rodriguez-Fajardo, and A. Forbes, "A vector holographic optical trap," Sci. Rep. **8**, 17387 (2018).
[20]S. A. Syubaev, A. Y. Zhizhchenko, D. V. Pavlov, S. O. Gurbatov, E. V. Pustovalov, A. P. Porfirev, S. N. Khonina, S. A. Kulinich, J. B. B. Rayappan, S. I. Kudryashov *et al.*, "Plasmonic nanolenses produced by cylindrical vector beam printing for sensing applications," Sci. Rep. **9**, 19750 (2019).
[21]L. Sun, Y. Zhang, Y. Wang, Y. Yang, C. Zhang, X. Weng, S. Zhu, and X. Yuan, "Real-time subcellular imaging based on graphene biosensors," Nanoscale **10**, 1759–1765 (2018).
[22]G. Bautista, J.-P. Kakko, V. Dhaka, X. Zang, L. Karvonen, H. Jiang, E. Kauppinen, H. Lipsanen, and M. Kauranen, "Nonlinear microscopy using cylindrical vector beams: Applications to three-dimensional imaging of nanostructures," Opt. Express **25**, 12463–12468 (2017).
[23]Y. Zhang, J. Shen, C. Min, Y. Jin, Y. Jiang, J. Liu, S. Zhu, Y. Sheng, A. V. Zayats, and X. Yuan, "Nonlinearity-induced multiplexed optical trapping and manipulation with femtosecond vector beams," Nano Lett. **18**, 5538–5543 (2018).
[24]L. Novotny and B. Hecht, "Surface plasmons," Princ. Nano-Opt. **90**, 378 (2006).
[25]Y. Kozawa and S. Sato, "Generation of a radially polarized laser beam by use of a conical Brewster prism," Opt. Lett. **30**, 3063–3065 (2005).
[26]M. A. Ahmed, A. Voss, M. M. Vogel, and T. Graf, "Multilayer polarizing grating mirror used for the generation of radial polarization in Yb:YAG thin-disk lasers," Opt. Lett. **32**, 3272–3274 (2007).
[27]D. N. Naik, N. A. Saad, D. N. Rao, and N. K. Viswanathan, "Ultrashort vortex from a Gaussian pulse—An achromatic-interferometric approach," Sci. Rep. **7**, 2395 (2017).
[28]Q. Zhan and J. R. Leger, "Interferometric measurement of the geometric phase in space-variant polarization manipulations," Opt. Commun. **213**, 241–245 (2002).
[29]K. Sueda, G. Miyaji, N. Miyanaga, and M. Nakatsuka, "Laguerre-Gaussian beam generated with a multilevel spiral phase plate for high intensity laser pulses," Opt. Express **12**, 3548–3553 (2004).
[30]S. M. Kamali, E. Arbabi, A. Arbabi, and A. Faraon, "A review of dielectric optical metasurfaces for wavefront control," Nanophotonics **7**, 1041–1068 (2018).
[31]N. Yu and F. Capasso, "Flat optics with designer metasurfaces," Nat. Mater. **13**, 139–150 (2014).
[32]H.-X. Xu, L. Zhang, Y. Kim, G.-M. Wang, X.-K. Zhang, Y. Sun, X. Ling, H. Liu, Z. Chen, and C.-W. Qiu, "Wavenumber-splitting metasurfaces achieve multichannel diffusive invisibility," Adv. Opt. Mater. **6**, 1800010 (2018).
[33]H. X. Xu, G. Hu, Y. Li, L. Han, J. Zhao, Y. Sun, F. Yuan, G. M. Wang, Z. H. Jiang, X. Ling *et al.*, "Interference-assisted kaleidoscopic meta-plexer for arbitrary spin-wavefront manipulation," Light: Sci. Appl. **8**, 3 (2019).
[34]A. I. Kuznetsov, A. E. Miroshnichenko, M. L. Brongersma, Y. S. Kivshar, and B. Luk'yanchuk, "Optically resonant dielectric nanostructures," Science **354**, aag2472 (2016).
[35]S. Kruk, B. Hopkins, I. I. Kravchenko, A. Miroshnichenko, D. N. Neshev, and Y. S. Kivshar, "Invited article: Broadband highly efficient dielectric metadevices for polarization control," APL Photonics **1**, 030801 (2016).
[36]J. M. López-Téllez, N. C. Bruce, J. Delgado-Aguillón, J. Garduño-Mejía, and M. Avendaño-Alejo, "Experimental method to characterize the retardance function of optical variable retarders," Am. J. Phys. **83**, 143–149 (2015).